



Review

Deformation Processes, Textural Evolution and Weakening in Retrograde Serpentinites

Cecilia Viti ^{1,*}, Cristiano Collettini ² , Telemaco Tesei ³, Matthew S. Tarling ⁴
and Steven A.F. Smith ⁴ 

¹ Dipartimento di Scienze Fisiche, della Terra e dell'Ambiente, Università di Siena, 53100, Italy

² Dipartimento di Scienze della Terra, La Sapienza Università di Roma, Piazzale Aldo Moro 5, 00185 Roma, Italy; cristiano.collettini@uniroma1.it

³ Department of Earth Sciences, Durham University, Elvet Hill, Durham DH1 3LE, UK; telemaco.tesei@ingv.it

⁴ Department of Geology, University of Otago, 360 Leith Street, 9016 Dunedin, New Zealand; tarma723@student.otago.ac.nz (M.S.T.); steven.smith@otago.ac.nz (S.A.F.S.)

* Correspondence: cecilia.viti@unisi.it

Received: 30 March 2018; Accepted: 31 May 2018; Published: 5 June 2018



Abstract: Serpentinites play a key role in controlling fault rheology in a wide range of geodynamic settings, from oceanic and continental rift zones to subduction zones. In this paper, we provide a summary of the most common deformation mechanisms and frictional strengths of serpentine minerals and serpentinites. We focus on deformation mechanisms in retrograde serpentinites, which show a progressive evolution from undeformed mesh and bastite pseudomorphic textures to foliated, ribbon-like textures formed by lizardite with strong crystallographic and shape preferred orientations. We also discuss the possible mechanical significance of anastomosing slickenfibres containing ultraweak fibrous serpentines or relatively strong splintery antigorite. Our review and new observations indicate that pressure solution and frictional sliding are the most important deformation mechanisms in retrograde serpentinite, and that they are frictionally weak ($\mu \sim 0.3$). The mineralogical and microstructural evolution of retrograde serpentinites during shearing suggests that a further reduction of the friction coefficient to μ of 0.15 or less may occur during deformation, resulting in a sort of continuous feedback weakening mechanism.

Keywords: retrograde serpentinite; slickenfibres veins; (001) sliding; pressure solution; brittle–ductile deformation; friction coefficient; weakness

1. Introduction

Serpentinites are among the most important components of the oceanic lithosphere, in the hydrated mantle wedge above subducting slabs, and in ophiolite sequences and ultramafic bodies within the continental crust. Due to their unique physical and rheological properties, serpentinites play a fundamental role in a wide range of geodynamic processes, ranging from fault zone weakening and aseismic creep along major fault zones at shallow depths (e.g., [1–6]) to high-temperature dehydration embrittlement and seismogenesis in subduction zones (e.g., [7–10]). Several recent papers have provided thorough reviews of the mechanical properties, deformation mechanisms and tectonic significance of serpentinite (e.g., [11–14]).

An understanding of the mechanical behaviour of serpentinite has been gained by combining geological and petrological studies of natural serpentinite-bearing faults and shear zones (e.g., [15–22]), with the results of deformation experiments designed to replicate a wide range of conditions, from the shallow crust up to ~ 8 GPa and 800 °C (e.g., [23–27]). Previous experimental studies have been performed on both serpentinitic rocks and serpentine minerals (that is, almost monomineralic

samples of lizardite, chrysotile and antigorite). The extremely different strain rates (10^{-4} – 10^{-5} s $^{-1}$ vs. 10^{-13} – 10^{-15} s $^{-1}$) and sample volumes (mm 3 vs. m 3 –km 3) involved in deformation experiments and natural shear zones [14] led to some discrepancies between experimental and natural observations concerning the most important deformation processes in serpentinite shear zones.

A straightforward comparison of mechanical data from different experiments is also hindered by the fact that natural serpentinites are very complex geological materials. Although serpentinite is often (incorrectly) considered to be a relatively “simple” monomineralic rock, it is well known that the serpentine family includes an extraordinarily wide range of minerals, including lizardite, chrysotile, antigorite and many other common varieties such as polygonal and polyhedral serpentines (e.g., [28,29]). Serpentine minerals share similar chemical compositions (typically close to the Mg end-member) and are all based on stacked tetrahedral and octahedral (TO) layers. However, differences in the crystal structure of the various serpentine minerals have unexpectedly strong effects on the overall mechanical behaviour. For example, natural and experimental observations indicate that serpentinites in which lizardite is the prevailing phase display different frictional strength and deformation mechanisms compared to those in which chrysotile or antigorite prevail (e.g., [6,21,30]).

In serpentinitic rocks, different serpentine minerals often coexist in chaotic ultrafine associations. In such cases, targeted microstructural and mineralogical investigation (e.g., through TEM or modern techniques of Raman spectroscopy (e.g., [31])) is the only way of correctly deciphering the rock mineralogy and micro-to-nanostructure. To complicate matters further, relict minerals (e.g., olivine, pyroxenes, and primary spinel) or minerals formed during serpentinitisation (e.g., magnetite and brucite) and metasomatism (e.g., talc, tremolite, and smectites) are commonly present in variable amounts, potentially modifying the overall fault rock texture and mechanical behaviour (e.g., [4,5,32,33]).

A further source of complexity is represented by rock microstructural variability. In the absence of deformation, serpentinites are fine- to ultrafine-grained and can be considered as mostly isotropic rocks. Two main microstructural “end members” of serpentinitic rocks can be distinguished (e.g., [34]): (1) retrograde pseudomorphous serpentinites (mostly consisting of lizardite, fibrous and poorly crystalline serpentines); and (2) prograde interpenetrating or interlocking serpentinites (mostly consisting of antigorite lamellae). However, during deformation in faults and shear zones, both microstructural “end members” evolve towards foliated serpentinites, and shape and lattice preferred orientations can be achieved through various deformation mechanisms. It is therefore evident that the overall mechanical behaviour of a serpentinite-bearing fault rock is determined by a complex interplay between the evolution of mineralogical and microstructural features. For this reason, an accurate mineralogical and micro-to-nanostructural characterisation of serpentinite samples should be considered a necessary prerequisite for correct sample identification and subsequent data interpretation.

The present paper focuses mainly on the deformation of retrograde pseudomorphous serpentinites, since they represent the most common type of serpentinite in the oceanic lithosphere, particularly in slow to ultraslow spreading ridges (e.g., [35]) and along oceanic transform faults (e.g., [36,37]). Moreover, they are also present in faults and shear zones in ophiolites on continents (e.g., [38–40] and references therein). The paper will report: (1) a brief summary of the main deformation mechanisms in serpentine minerals and serpentinites, with a focus on brittle and brittle–ductile deformation in the upper crust; (2) an overview of the frictional strengths of serpentine minerals and serpentinites; (3) a detailed description of the deformation mechanisms in pseudomorphous serpentinites; and (4) a summary of some of the main geodynamic implications, with specific reference to the potential weakening behaviour of retrograde serpentinites.

2. Main Deformation Mechanisms in Serpentine Minerals and Serpentinites

Depending on the pressure–temperature conditions, stress field, strain rate and intrinsic properties of the sample (e.g., mineralogy and microstructure), serpentinites can show brittle, intermediate brittle–ductile or fully ductile deformation. Here we focus on brittle fracturing and delamination

along (001) planes, frictional sliding along (001) planes, and pressure solution creep, because these are among the most commonly observed deformation mechanisms in both naturally and experimentally deformed retrograde serpentinites over a wide range of geological conditions.

2.1. Brittle Fracturing, Cataclasis and Grain Size Reduction

A recent overview of the mechanical behaviour of serpentine was provided by Amiguet et al. [13] who performed deformation experiments on samples of lizardite and antigorite at high P (1–8 GPa), high T (150–500 °C) and strain rates in the range of 10^{-4} – 10^{-6} s⁻¹. Their experimental data indicated that in lizardite, the brittle–ductile transition occurs at relatively shallow depths (ca. 10 km) at a pressure of ca. 300 MPa. In their experiments, this transition occurred at a shear stress of ca. 100 MPa. In the brittle regime, lizardite deforms mainly by microcracking along (001) planes as a consequence of weak interlayer hydrogen bonds (e.g., [24]). In the ductile regime, grain size reduction parallel to grain boundaries is facilitated by kinking and preferential gliding along the basal (001) plane. In antigorite, the brittle–ductile transition occurs at much higher pressures (~1 GPa) than lizardite, equivalent to a depth of ~30 km. Deformation occurs by preferential microfracturing along conjugate (101) and ($\bar{1}0\bar{1}$) planes, which are the most weakly bonded planes in the antigorite structure. In the experiments of [13], microfracturing resulted in interconnected regions with intense grain size reduction, but similar regions are not frequently observed in naturally deformed lizardite and antigorite. This may reflect the dominance of other deformation mechanisms such as pressure solution in natural serpentinite samples, even in those deformed at low T (e.g., [41]).

Brittle fracturing and cataclasis do not appear to be important processes in natural serpentinites, especially in retrograde lizardite-rich serpentinites where they are only observed to occur at very shallow depths in correspondence to the latest tectonic activity. At the mesoscale, brittle deformation of retrograde serpentinites typically results in the formation of metre-scale tabular layers of incohesive gouge along late-stage faults (e.g., [17,18]), or thinner gouges layers along the boundaries between massive serpentinite and shear veins [19,42]. Brittle fracturing is expected to be more frequent in interpenetrating/interlocking prograde serpentinites due to the higher pressures required to reach the brittle–ductile transition in antigorite (e.g., [13,14,43]), but again it is not frequently described in natural samples. Instead, brittle fracturing is commonly observed in partially serpentinised peridotites, where fractures easily propagate at serpentine-olivine and serpentine-pyroxene grain boundaries [17]. Brittle fracturing is a fundamental process in the early stages of peridotite serpentinisation, because, by increasing rock permeability, it promotes the formation of fluid pathways and allows for efficient interface reactions between serpentine and primary minerals in peridotite (e.g., [44]). Brittle fracturing can be enhanced by the solid volume increase during serpentinisation reactions [45–47].

We recommend that the terms “grain size reduction” and “microcracking/delamination along (001)” are carefully distinguished in the case of serpentines (and other layer silicates) because the two mechanisms give rise to different microstructures and mechanical properties (Figure 1a).

Microcracking and delamination along basal planes of serpentine single crystals favour sliding along (001) planes, which may represent the predominant and pervasive deformation mechanism in lizardite-rich serpentinites characterised by shape and crystallographic preferred orientations (SPO and CPO, respectively). Brittle fracturing along planes other than (001) results in “true” grain size reduction, which favours cataclastic flow along fine-ultrafine cataclastic shear bands. Together with their different mechanical behaviour, the two cases (delamination vs. single crystal fracturing) would also correspond to different reactivity and different response in terms of fluid–rock interaction and fluid circulation. In the case of bastites, which are polycrystalline lamellar aggregates (up to cm in size) formed by different serpentines in random and ultrafine associations (Figure 1b), brittle deformation does not result in grain/crystal size reduction but in the formation of polycrystalline clasts tens to hundreds μ m in size. Preferential cataclastic flow may progressively reduce the size of the clasts down to the single crystal size (nanoscale).

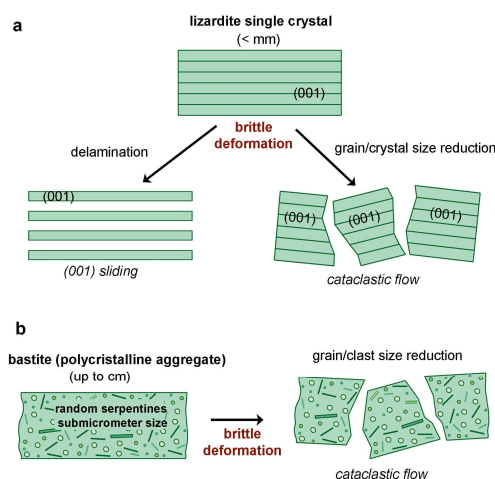


Figure 1. The effects of brittle deformation in: (a) serpentine single crystal (lizardite); and (b) serpentine polycrystalline aggregate (e.g., a bastitic lamella). (001) delamination favours easy (001) sliding in foliated lizardite-rich serpentinite, whereas grain-, crystal- or clast-size reduction favours cataclastic flow.

2.2. Easy Sliding Along (001)

Many papers describe (001) sliding as a fundamental deformation mechanism in serpentine minerals, and suggest that it can explain ductile behaviour in both natural and experimental samples (e.g., [13,27,48]). As previously anticipated, preferential microfracturing and slipping planes coincide in lizardite, and correspond to basal (001) planes, with [100] as the preferred slip direction. In the case of antigorite, combined slip along (101) and $(10\bar{1})$ microfracturing planes results in an apparent global slip along (001), thus with an overall behaviour similar to lizardite, so that Figure 1a can be also applied to antigorite single crystals. However, there is not full agreement in the literature about the preferential slip direction in antigorite, and both [100] and [010] have been proposed (e.g., Amiguet et al. [13] and Campione et al. [49], respectively).

A critical feature is that (001) sliding has significant rheological effects only if lizardite and antigorite crystals have a SPO and LPO, allowing pervasive and interconnected sliding across the serpentinite mass. In interpenetrating and interlocking antigorite serpentinites, LPO can be attained by rotation and alignment of previously formed antigorite crystals or by synkinematic growth of antigorite. In retrograde lizardite-rich serpentinites, LPO is formed mainly by pressure solution and re-precipitation processes as detailed below.

2.3. “Fibre on Fibre” Sliding Mechanism in Fibrous Serpentine

Many natural occurrences of highly deformed serpentinites are dominated by chrysotile or other fibrous serpentines [21,34,50]. In such cases, the serpentine fibres are typically strongly aligned parallel to the transport direction, giving rise to extremely strong anisotropy and schistosity (e.g., [19,21]). The rolled structure of chrysotile or the sectorial arrangement of polygonal serpentine exclude (001) sliding mechanisms, as well as easy sliding along other crystallographic planes. Instead, we suggest that a “fibre on fibre” sliding mechanism could explain the extreme weakness of shear zones formed mainly by isoriated chrysotile fibres. The frictional strength of chrysotile is described below.

2.4. Dissolution and Precipitation

At relatively low temperatures, dissolution–precipitation is often the predominant deformation mechanism in serpentinites, acting in concert with (001) sliding (e.g., [17,22,51–53]). Most studies deal with retrograde serpentinites and highlight that dissolution and precipitation processes have two main effects: firstly, they induce significant mineralogical and microstructural changes in massive serpentinites and, secondly, they result in the formation of fibrous veins filled by newly-precipitated serpentine. Chrysotile-rich veins and shear zones often occur so pervasively within serpentinite

outcrops that the term “chrysotile schistosity” has been used to describe such occurrences. For example, Andreani et al. [19] described the formation of foliated serpentinite by dissolution and synkinematic crystallisation of isoriented chrysotile fibres. These authors suggested a first step involving brittle microfracturing and fluid circulation, followed by dissolution at highly-stressed clast contacts by pressure-solution. They also observed that mass transfer occurs over short distances, so that dilatant sites that form around clasts, are continuously filled by newly-formed chrysotile fibres. Fibre orientation in such cases is influenced by local shearing direction and clast rotation. Similar findings were also reported in papers (e.g., [21,34]) that describe the progressive evolution from blocky serpentinites to chrysotile schists by replacement of previous serpentines and subsequent precipitation of chrysotile.

Fully hydrated undeformed serpentinites, as well as foliated serpentinites, show limited cataclastic deformation and are usually considered as effective fluid barriers. Experimental measurements of permeability in antigorite-rich samples have yielded permeabilities ranging from 10^{-18} to 10^{-22} m² [54,55]. The lowest permeabilities were measured at higher confining pressures (50 MPa in the experiments) when microcracks were closed and fluid flow occurred through pores and along grain boundaries. These results suggest that natural serpentinite fault rocks have extremely low permeability and that fluid circulation will be limited. However, recent studies have demonstrated that in fully hydrated serpentinites fluid circulation is facilitated by micro-to-nanoscale interconnected porosity [44,56,57], possibly suggesting that pervasive microfracturing is not necessary for fluid flow during pressure-solution deformation. In retrograde serpentinites, nanoporosity can be localised within pseudomorphic sites containing randomly oriented mixtures of ultrafine serpentine fibres and lamellae (i.e., mesh cores and bastites). Nanoporosity and ultrafine grain sizes may enhance fluid/rock interaction and dissolution processes, meaning that these pseudomorphic sites are more prone to pressure solution processes.

3. Friction Coefficients of Serpentine Minerals and Serpentinites

The frictional strength of serpentinites over a wide range of conditions is still debated, partly because experimental measurements of the friction coefficient of different serpentine varieties do not reveal a consistent picture (Figure 2a).

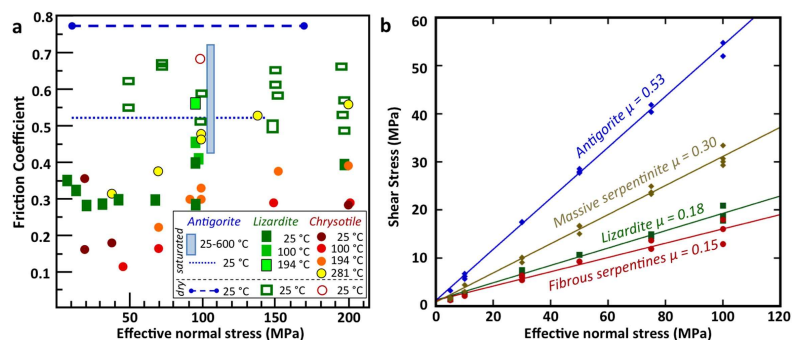


Figure 2. Summary of frictional strength of serpentine minerals. (a) Friction coefficient vs. effective normal stress for the three main varieties of serpentine minerals. Lizardite data (squares) have been compiled from [58] and references therein, and from [59]. Chrysotile data (circles) compiled from [60]. Antigorite data at room temperature represent the failure envelopes presented in Dengo et al. [61] and Tesei et al. [62] for dry precut cylinders (bold dashed line) and saturated fault gouges (thin dashed line), respectively. Friction of antigorite at variable temperature (light blue square) compiled from [63]. (b) Failure envelopes and friction coefficients of experimental serpentine fault gouges, modified from Tesei et al [62]. All tests were carried out at room temperature, saturated conditions and steady-state sliding velocity of 10 $\mu\text{m/s}$, in a direct shear configuration. The slope of the linear fit represents the average coefficient of friction.

It is generally accepted that antigorite is relatively strong (friction coefficient, μ , from 0.45 to 0.85) over a wide range of temperatures and in both dry and wet conditions [1,30,61,63]. Chrysotile is typically described as the weakest serpentine mineral ($\mu \sim 0.2$; e.g., [64]), but it shows a strong temperature dependence, becoming much stronger above 200 °C [2,58,60,65]. The frictional strength of lizardite is more poorly constrained, with friction coefficients ranging from 0.15 to 0.80 [4,30,58,61,65,66], even if the lowest value (0.15) was actually referred to a chrysotile sample. Based on these experimental data, it has been concluded that serpentine alone cannot explain the extreme long-term weakness of faults such as the San Andreas, and that other weak minerals commonly associated with serpentine, such as smectites or talc, have to be considered (e.g., [2,5,67,68]). One of the problems in evaluating the frictional strength of serpentinites is that the starting materials for experiments are often mixtures of different serpentine varieties, and determination of the mineralogical “purity” is a complicated and time-consuming problem requiring careful analytical work (e.g., TEM). Recently, Tesei et al. [62] tested a suite of well-characterised and almost pure serpentine samples that can be considered as a sort of “mechanical end members” in the complex range of serpentine frictional properties. The authors investigated crystalline lizardite, fibrous serpentine (chrysotile and polygonal serpentine mixtures) and antigorite from shear veins exposed on the Island of Elba (Italy), together with a representative sample of undeformed retrograde serpentinite (samples details in [28,69–71]). In their experiments (Figure 2b), antigorite showed a relatively high friction coefficient, $\mu = 0.53$, consistent with previous literature, whereas both lizardite and fibrous serpentine were frictionally weak at temperatures up to ~ 170 °C. As expected, mixtures of chrysotile and polygonal serpentine showed a very low frictional strength ($\mu = 0.15$), possibly due to the easy “fibre on fibre” sliding mechanism described earlier. This mechanism is enhanced by the fact that, during the experiments, chrysotile and polygonal serpentine fibres quickly develop a shear fabric of well-oriented fibres parallel to the shear direction. Pure lizardite showed a frictional strength much lower than previously reported, with a friction coefficient of $\mu = 0.18$. The different frictional strengths of lizardite and antigorite are most likely related to the relative ease of (001) sliding, which is accomplished more readily in lizardite (weak hydrogen bonds in the interlayer) than in antigorite (stronger bonds due to tetrahedral inversions). Experiments carried out at $T \sim 170$ °C on fibrous serpentine and lizardite gouges revealed that the strength of these minerals is not affected by temperature increase, and that they remain very weak with $\mu = 0.19$ and $\mu = 0.18$, respectively, at elevated temperatures. Based on the experiments of Tesei et al. [62], lizardite, chrysotile and polygonal serpentine are all frictionally weak varieties of serpentine ($\mu \sim 0.2$ or lower), whereas antigorite is frictionally strong. Building on this experimental evidence and considering the crystalline structure of conical-, polyhedral-, and proto-serpentine, it seems likely that also these varieties possess a low frictional strength, although this remains to be validated with experimental data.

Friction experiments on the sample of undeformed retrograde serpentinite (see below for mineralogical and microstructural description) showed a friction coefficient of $\mu = 0.30$ [62]. This result is in good agreement with Escartin et al. [24] who deformed similar samples at pressures of up to 400 MPa (i.e., lizardite-rich, mesh-textured serpentinites). This friction value is slightly higher than those obtained for pure lizardite and fibrous serpentines, which are the main rock-forming phases in the tested sample. This discrepancy could be due to the occurrence of other phases in the retrograde serpentinite, including magnetite that is arranged in a reticulate pattern along rim/rim boundaries. Alternatively, it may be because the monomineralic samples can more easily evolve shape and crystallographic preferred orientations during the experiments. The friction coefficient of the undeformed retrograde serpentinites ($\mu \sim 0.3$) is sufficiently low enough to explain strain localisation and fault weakness in a range of tectonic settings (e.g., [12,14,48]). Additionally, once deformation starts, the progressive mineralogical and microstructural evolution from retrograde to foliated serpentinites may further reduce the overall frictional strength by forming highly interconnected and aligned lamellae of serpentine. The following paragraphs focus on the mineralogical and microstructural changes that take place during the transition from massive retrograde to foliated serpentinites.

4. A Focus on Deformation in Retrograde Serpentinities

4.1. The Starting Material: Retrograde Pseudomorphic Serpentinities from the Meso- to the Nano-Scale

Our samples of retrograde serpentinites come from Southern Tuscany (Italy) and belong to the Internal Ligurid Unit [72,73]. At the mesoscale, these serpentinites exhibit characteristic structures that are common in many other retrograde serpentinites around the world. Such characteristics include the occurrence of dark green lenses of massive serpentinite that are highly variable in size and have a sigmoidal shape. The massive lenses are initially reduced in size by “brittle” fracturing and boudinage and evolve to a more foliated fabric over time. The lenses are enveloped by pale green, fibrous slickenfibres veins and green shiny coatings (Figure 3) that formed along a complex system of anastomosing faults.

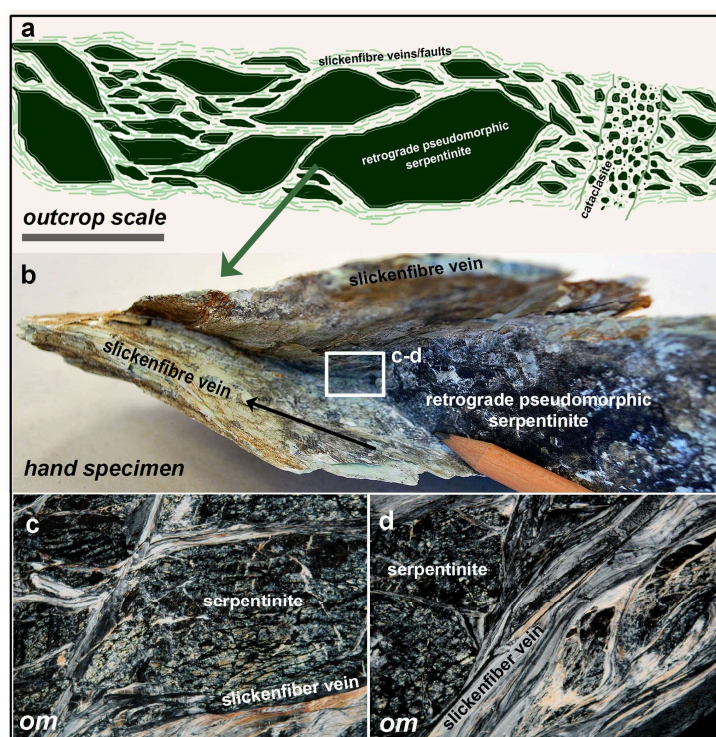


Figure 3. Common characteristics of retrograde serpentinite at a range of scales. (a) Dark-green lenses of massive serpentinite surrounded by pale-green, anastomosing slickenfibres-coated faults. Cataclasites are localised along late-stage faults that crosscut the previously-formed fabrics. Scale bar corresponds to ~3 m. (b) Hand specimen showing the contact between a massive serpentinite lens and a slickenfibres veins. (c,d) Polarised-light images (crossed nicols) from the contact between massive mesh textured serpentinite and slickenfibres veins; these microstructures are consistent with a dominant pressure solution-precipitation process.

The veins often display “crack-seal” texture suggesting that precipitation of new serpentine occurred during incremental fault movement. As detailed above, these veins are considered to be one of the main products of dissolution-precipitation processes (see references above). Figure 3 also highlights that the overall arrangement of lens-shaped massive serpentinites and slickenfibres veins is maintained from the mesoscale down to the microscale. Serpentine cataclasites (Figure 3a, right side) occur along fault zones that crosscut earlier-formed fabrics, and are probably related to the latest phase of tectonic activity.

From a mineralogical point of view, retrograde serpentinites in massive lenses consist mainly of fibrous and poorly crystalline serpentines, lizardite and magnetite. Relict olivine, pyroxene and spinel,

as well as secondary chlorite, “ferritchromit” aureoles and hydrogarnets may occur as minor phases. In the absence of deformation, pseudomorphic serpentinites can be considered as isotropic rocks formed by a “mesh-textured” matrix which hosts isolated bastitic lamellae. The meshes usually show distinct cores and rims (Figure 4a,c). Bastites and mesh cores are mineralogically equivalent, consisting of mixtures of different serpentine minerals (chrysotile, polygonal serpentine, protoserpentine, and tiny lamellae of lizardite). In mesh cores, serpentines occur in completely random orientation, whereas, in bastites, isororiented lizardite lamellae (a few nm thick) may be intercalated to randomly oriented serpentines. Mesh rims represent the most crystalline sites, consisting of up to micrometre-sized lizardite sectors with their [001] axes perpendicular to the core/rim boundaries [71]. In meshes, lizardite therefore occurs mainly in two orientations, as highlighted by using the retardation plate in the petrographic microscope (e.g., Figure 4b,d,e). Lizardite (001) planes are broadly maintained from one mesh to another (Figure 4b,d,f) resulting in an interconnected 3D network with two broadly perpendicular CPOs.

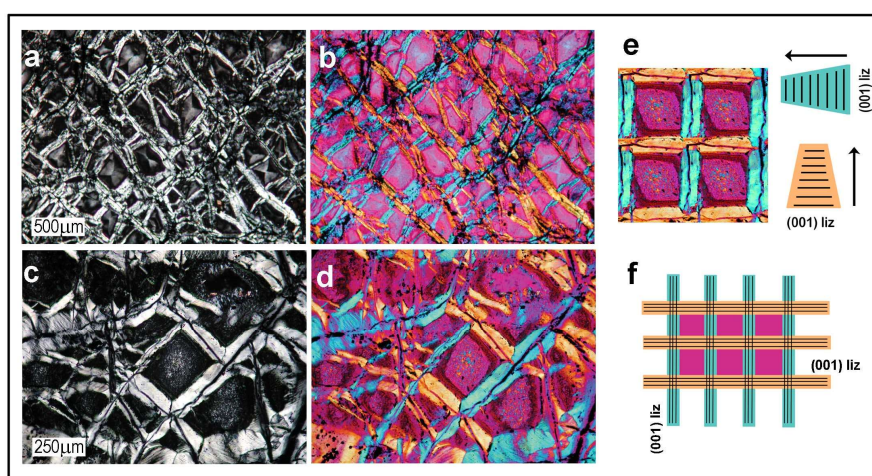


Figure 4. Microstructures of undeformed mesh textures: (a,c) Polarised-light images of undeformed mesh textures (crossed nicols). (b,d) Corresponding images with the retardation gypsum plate show pink-reddish cores formed by poorly crystalline random mixtures, and yellow/blue lizardite rims. (e) Four mesh cells (elaborated from (d)) showing the two main orientations of (001)_{liz} in rims (here, vertical in “blue” and horizontal in “yellow” rims). (f) 2D cartoon showing the occurrence of a sort of “crossed” CPO, with two main (001)_{liz} orientations.

In undeformed pseudomorphic serpentinites, the thickness of “blue” and “yellow” rims is similar throughout the rock, and the volume occupied by the cores (pink-reddish in Figure 4b,d) is larger than that occupied by the rims. As described below, these subtle mineralogical and microstructural differences among pseudomorphic sites significantly affect the local strength of the retrograde serpentinite, resulting in an inhomogeneous response to stress. We remark that this kind of sample has provided friction coefficient of 0.3 (see above).

4.2. Stress Response in Retrograde Pseudomorphic Serpentinites

4.2.1. Deformation Mechanisms in Mesh Textured Serpentinites

Understanding the behaviour of mesh textures during deformation is important for two main reasons: (1) meshes occupy most of the volume of retrograde serpentinites; and (2) in contrast to bastites that occur as isolated lamellae, meshes form an interconnected 3D framework and therefore control the distribution of stress in retrograde serpentinites. Figure 5 shows the typical microstructure of meshes in highly deformed serpentinites.

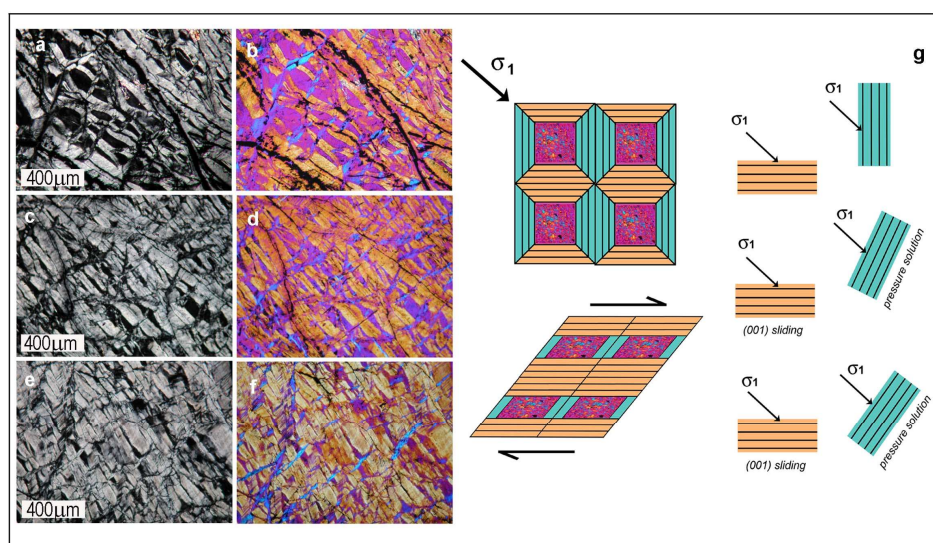


Figure 5. Progressive deformation of mesh textures: (a,c,e) polarised-light images (crossed nicols) showing progressive deformation of mesh textures until the cores disappear; (b,d,f) corresponding images with the retardation gypsum plate; and (g) cartoon showing stress response in four mesh cells. The cartoon shows the orientation of σ_1 with respect to $(001)_{\text{liz}}$ in rims. It is worth noting that, during shear deformation, the angle between σ_1 and $(001)_{\text{liz}}$ of blue rims progressively increases, whereas it remains constant in the case of yellow rims.

The ideally square-shaped cells (Figure 4) evolve to lens-shaped, sigmoidal cells, showing a progressive reduction of the core volume until it completely disappears (e.g., Figure 5e). This texture has been reported as “ribbon texture” in the literature, after the terminology used to describe ductile fabrics in mylonites (e.g., [15]). However, the most likely deformation mechanism in mesh cores is pressure solution, and the preferential disappearance of cores with respect to nearby rims is probably a consequence of their higher porosity and ultrafine grain size, which may result in localised fluid circulation and enhanced reaction kinetics. Alternatively, Hirauchi et al. [27] reported that grain boundary sliding in fine- to ultrafine-grained cores is another viable mechanism of deformation, at least under relatively fast strain rates ($\epsilon \sim 3 \times 10^{-4} \text{ s}^{-1}$).

In deformed samples, the two set of mesh rims (Figure 5b,d,f) display a different stress response. In particular, one set of rims (here, the “blue” lizardite) is reduced in size, whereas the other set (the “yellow” lizardite) is well preserved and may increase in thickness. The different response of lizardite crystals in the two sets of rims is related to the orientation of the maximum principal stress (σ_1) and the shear direction. To illustrate this effect, Figure 5g shows the relationship between the mesh textures and σ_1 during shearing. At the onset of deformation, the orientation of σ_1 with respect to the (001) planes of the “blue” and “yellow” lizardite is the same. However, as deformation continues and the meshes are progressively sheared and/or rotated, the angle between σ_1 and the “blue” lizardite (001) progressively increases, whereas it remains the same for “yellow” lizardite. In this case, the blue rims are probably exposed to greater stress, favouring pressure solution instead of sliding along (001) . In contrast, frictional sliding may be the predominant deformation mechanism for the yellow lizardite that has an orientation favouring easy (001) glide. In highly deformed serpentinite, yellow rims evolve to an interconnected network of sub-parallel ribbons (e.g., Figure 5e,f). Ultimately, the undeformed isotropic serpentinite evolves to a highly foliated and sheared fault rock, mostly formed by lizardite crystals (yellow) with both a well-defined SPO (subparallel ultrathin lamellae) and strong CPO (subparallel (001) planes). Considering the low friction coefficient of lizardite ($\mu = 0.18$), easy sliding along (001) planes parallel to the shear direction represents an efficient weakening mechanism in sheared serpentinites dominated by lizardite. Progressive sliding also results in extreme delamination

of lizardite lamellae, with thickness reduction down to the nanoscale. Similar microstructures have been observed in high strain ($P = 1$ GPa and $T = 200$ °C; $\gamma \sim 4$ – 6) deformation experiments performed on mesh-textured serpentinites by Hirauchi et al. [27], who describe pervasive (001) glide of lizardite sectors, as well as in natural samples by Maltman [15], who described the deformation-induced evolution from mesh to ribbon textures.

4.2.2. Deformation Mechanisms in Bastites

Bastites are serpentine pseudomorphs formed by hydration of pyroxenes and consist of polycrystalline aggregates of different serpentine varieties. The mineralogical and nanotextural characteristics of bastites are similar to those of mesh cores. Bastitic lamellae in a single sample may show evidence of both brittle deformation (e.g., microfractures and microfaults; Figure 6a,b) and ductile deformation (e.g., microfolds and kinks; Figure 6c,d), resulting in disaggregation and pseudomorph grain-size reduction.

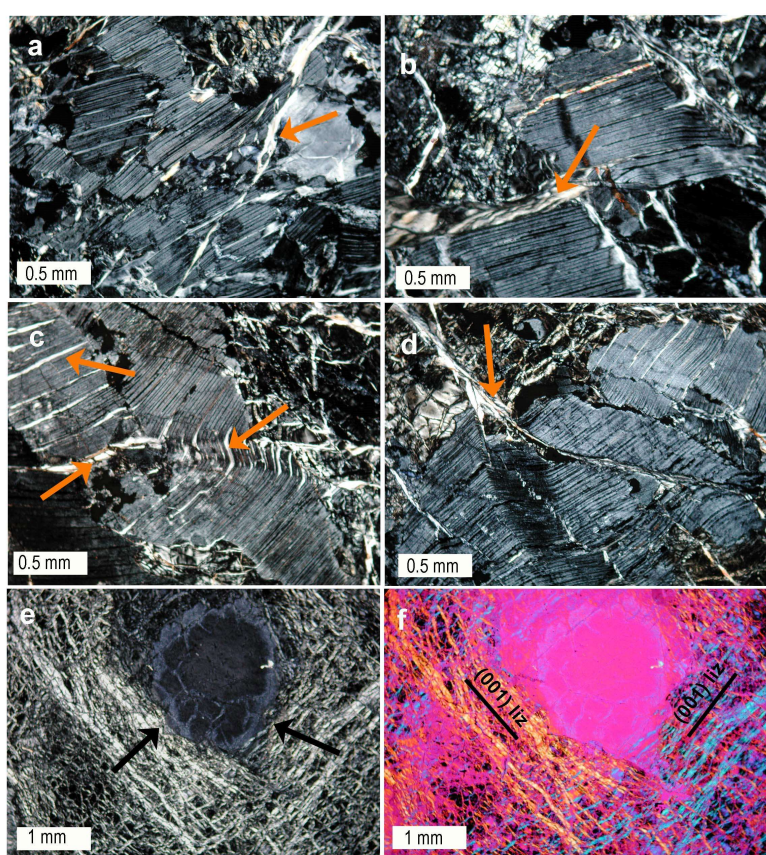


Figure 6. Deformation microstructures in bastites (polarised light images, crossed nicols). (a,b) Brittle fracturing of bastitic lamellae, with disaggregation and polymorph grain-size reduction. Note that bastites are crosscut by chrysotile veinlets (orange arrows). (c,d) Folding and kinking in bastitic lamellae, highlighted by the traces of pyroxene cleavage planes. Cleavage traces are typically filled by chrysotile veinlets that favour cleavage-parallel sliding of bastite “slices”. (e) Influence of bastite on the deformation of surrounding meshes. Black arrows indicate local overstress at the bastite edges on nearby mesh cells. (f) Corresponding image with the retardation gypsum plate, showing preferential dissolution of lizardite sectors with (001) planes perpendicular to bastite edges.

This disaggregation process is enhanced by the pervasive occurrence of chrysotile veinlets (orange arrows in Figure 6a–d), often oriented parallel to the original traces of pyroxene cleavage, allowing easy sliding of the bastite fragments/clasts.

Since the mineralogy and micro/nanostructures of bastites are broadly equivalent to those of mesh cores, we should expect a similar preference for pressure solution processes. During deformation, bastitic lamellae may locally affect the interplay between preferential pressure solution and (001) sliding in nearby sets of lizardite rims (Figure 6e). In particular, Figure 6f shows how the preferential dissolution of “yellow” vs. “blue” lizardite crystals may locally change due to the occurrence of bastite, which may induce local stress concentration (unrelated to σ_1) and preferential dissolution of those rims with (001)_{liz} perpendicular to the bastite boundary. In highly deformed serpentinites, bastites show progressive disaggregation and more rounded boundaries. This suggests progressive microfracturing, detachment and grain boundary sliding, as well as preferential dissolution of stressed serpentine grains at bastite boundaries. The most strongly foliated serpentinites usually do not maintain traces of bastitic lamellae.

5. The Role of Serpentine Veins

Serpentine veins and slickenfibres-coated fault surfaces are widespread in all serpentinitic outcrops, and are interpreted as one of the main products of the pressure solution and re-precipitation process. Andreani et al. [74] described the kinetic control on serpentine vein mineralogy, with an overall chronological evolution from poorly crystalline protoserpentine to conical serpentine, chrysotile, polygonal serpentine, polyhedral serpentine and lizardite. According to these authors, the main serpentine veins found in natural faults and shear zones are (formed from the first to last stages of serpentinite evolution): isolated sigmoidal chrysotile veins (V2 in their classification); crack-seal veins formed by variable mixtures of protoserpentine, chrysotile and polygonal serpentine fibres (V3; see also [53] for this kind of vein); and polyhedral serpentine/lizardite veins (V4). Together with these varieties, we also remark that splintery antigorite slickenfibre veins are extremely widespread and that, quite surprisingly, they have remained relatively poorly described in recent studies [69,75,76].

At the outcrop scale, fibrous serpentine veins (type V3 in [74]) and splintery antigorite veins represent the most commonly encountered vein types. These veins often constitute the typical anastomosing slickenfibre faults that surround lens-shaped massive blocks (e.g., Figure 3). Fibrous serpentine veins and splintery antigorite veins are difficult to distinguish in outcrop or hand specimen because they show similar macroscopic characteristics and are often found in similar structural settings. Both are pale green-whitish in colour and strongly anisotropic, due to the preferred alignment of serpentine fibres and antigorite splinters parallel to the shear direction. However, the predominance of chrysotile in fibrous veins and antigorite in splintery veins implies that their frictional behaviour is definitely different.

5.1. Ultraweak Fibrous Serpentine Veins

Fibrous serpentine veins are mostly formed by chrysotile and polygonal serpentine in variable proportions. Based on the low friction coefficients of the constituent serpentine minerals, fibrous veins represent the weakest domains in serpentinitic outcrops, meaning that they can preferentially accommodate deformation by easy frictional sliding (e.g., [19,21]), possibly by a “fibre on fibre” slip mechanism. Fibre isorientation in veins indicates growth under synkinematic conditions, rather than reorientation of fibres [19], with the fibre axes subparallel to shear direction. The orientation of serpentine fibres may change sharply within a single vein (yellow arrows in Figure 7a,b), giving rise to overlapping slickenfibre “subveins”.

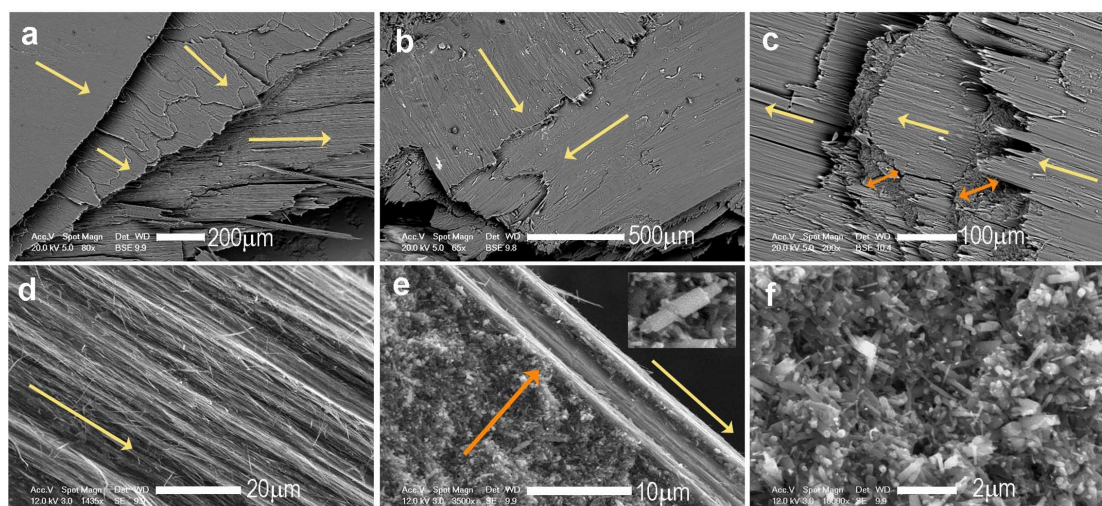


Figure 7. Back-scattered electron scanning electron microscope (BSE/SEM) images of slickenfibre veins and faults formed by fibrous serpentines (chrysotile and polygonal serpentine). (a,b) The yellow arrows highlight the sharp changes in fibre orientation in overlapping veins, probably reflecting local changes in shear direction. (c) Intercalation of fibrous veins with strongly oriented fibres (yellow arrows, mostly chrysotile) and randomly oriented fibres (orange arrows, mostly polygonal serpentine). (d) Detail of a slickenfibre surface, showing long fibres of chrysotile with preferred orientation parallel to shear direction. (e,f) Details of randomly oriented veins, characterised by the predominance of short fibres of polygonal serpentine; the inset in Figure 6e shows the typical habit of polygonal serpentine parallel to fibre axis (e.g., [28]).

Such variations do not necessarily correspond to “regional” tectonic changes in shear direction, but are related to local changes in shear direction arising from the relative movement of nearby lens-shaped blocks. Veins characterised by strongly aligned fibres may be also intercalated with other veins in which the fibres do not show preferential orientation (orange arrows in Figure 7c), the latter suggesting crystallisation in static conditions. Figure 7d shows a detail of a vein with strongly oriented fibres (predominantly chrysotile), whereas Figure 7e shows a cross-sectional view of a vein with intercalation of oriented and randomly oriented (orange arrow) fibrous serpentines. Figure 7e,f reveal that in random mixtures, polygonal serpentine prevails over chrysotile, probably due to more favourable kinetics, in agreement with [74].

5.2. The Puzzling Case of Antigorite Splintery Veins

Splintery antigorite veins have been described by Viti et al. [69] (and references therein), who studied a set of approximately 20 slickenfibre veins collected from different serpentinitic outcrops on the Island of Elba (see Figure 1 in Viti et al. [69] for sample location, and Bortolotti et al. [77] for geological map). TEM and electron diffraction studies revealed that splintery veins are almost exclusively formed by antigorite, with minor interstitial chrysotile fibres. The superstructure periodicity (corresponding to the wavelength of the antigorite corrugated crystal structure) obtained in the different veins was unrelated to regional and contact metamorphic grade, unlike what is reported for antigorite-bearing massive serpentinites (e.g., [78]). More recently, antigorite veins have been described by Groppo et al. [75] and Quesnel et al. [76], and similar occurrences may be found in asbestos-related studies, where the term “fibrous antigorite” is typically used. Antigorite crystals are highly elongated, parallel to the $[010]_{\text{atg}}$ axis. Splintery veins display CPO since all $[010]_{\text{atg}}$ axes are subparallel to the shear direction (Figure 8, orange arrows).

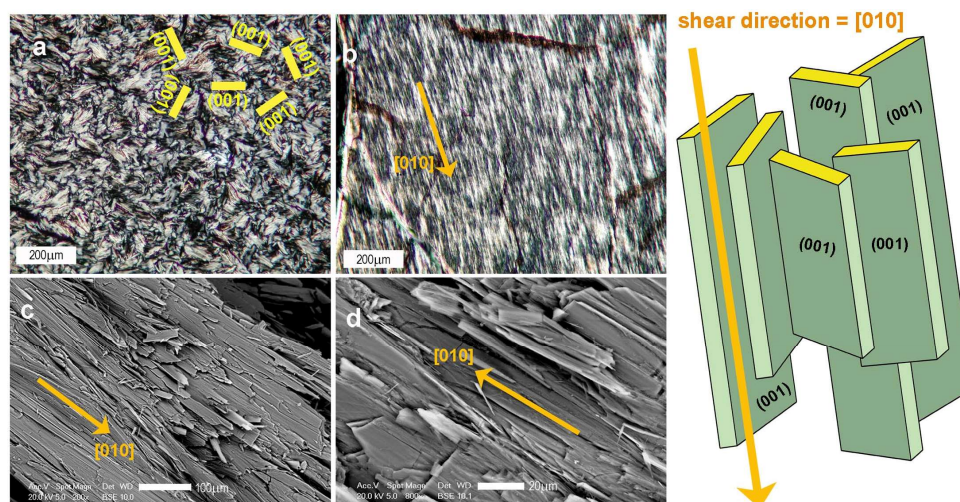


Figure 8. Splintery antigorite veins. (a and b) Polarised light images (crossed nicols) taken orthogonal (a) and parallel (b) to the splinter elongation direction. (c,d) BSE/SEM images of splintery antigorite veins; orange arrows indicate shear direction and correspond to antigorite [010]. The cartoon shows the shape and the crystallographic orientation of antigorite crystals in splintery veins, with [010] axes broadly parallel to the shear direction. In this orientation, the (001) planes of antigorite are randomly oriented around [010], but are parallel to the shear direction, potentially favouring strain-induced (001) sliding.

Perpendicular to the vein walls and the shear direction (i.e. orthogonal to $[010]_{\text{atg}}$ elongation axis; Figure 8a), antigorite splinters display rectangular cross sections (yellow in Figure 8a) with the long side corresponding to (001). Figure 8a shows that $(001)_{\text{atg}}$ are randomly oriented, with rotational disorder around [010]. Therefore, there is no preferred orientation of $(001)_{\text{atg}}$ planes, but we remark that all of them are parallel to the shear direction (Figure 8b–d and cartoon). The observed microstructure, based on $[010]_{\text{atg}}$ CPO and (001) planes rotated around [010] but parallel to shear direction, is consistent with (001) sliding, as suggested by previous papers on antigorite deformation mechanisms. The correspondence between the [010] axis and the shear direction would indicate [010] as the most suitable sliding direction, in agreement with [49].

An important question is: why this kind of slickenfibre fault is formed by antigorite rather than chrysotile and/or polygonal serpentine? Based on current understanding of serpentine stability fields (e.g., [79,80] and references therein), antigorite splintery veins are predicted to form at relatively higher temperature and metamorphic grade compared to fibrous serpentine veins. However, the coexistence of the two kinds of slickenfibre veins in outcrops where there is no clear correspondence between the occurrence of antigorite and prograde metamorphism in host serpentinites remains enigmatic.

We suggest two possible genetic mechanisms to explain the widespread occurrence of splintery antigorite veins, related to primary and secondary crystallisation. In the first case (primary crystallisation), vein antigorite is formed by solution and precipitation processes, following the same mechanism responsible for the formation of fibrous serpentine veins, but at slightly higher metamorphic grades. The precipitation of antigorite instead of chrysotile would be favoured at greater depths, possibly with circulation of hydrothermal fluids (higher T and silica content), lower fluid/rock ratios and slower crystallisation kinetics. During exhumation, the sluggish kinetics of the antigorite to chrysotile reaction may allow the preservation of antigorite under metastable conditions. The coexistence of chrysotile and antigorite veins in the same outcrop indicates that slickenfibre veins/faults were continuously formed during serpentinite emplacement under variable geological conditions, and that at shallower depths the crystallisation in veins and faults switched from antigorite to fibrous serpentines.

Alternatively, splintery antigorite veins could represent a “secondary” feature, resulting from the replacement of previously formed fibrous serpentine veins. Due to the coexistence of both varieties in the same outcrop, this hypothesis requires that the replacement of chrysotile by antigorite is not regionally controlled, but is triggered by local features acting on the single vein. A possible explanation could be local overstress resulting from the dynamic interplay of nearby massive blocks. Another possibility is represented by late-stage circulation of high-T, silica-rich hydrothermal fluids channelled along some of the pre-existing faults, as observed at mid-ocean ridge hydrothermal fields (e.g., [81]).

Whatever the mechanism to form splintery antigorite veins, the relatively high friction coefficient of antigorite (see references above) suggests that they represent the strongest domains within retrograde serpentinites, and contrast the ultraweak behaviour of fibrous serpentine veins. In fact, the observed micro-nanostructure of splintery veins is consistent with possible (001)_{atg} sliding, but this orientation does not correspond to the weakest surface in the antigorite crystal structure, meaning that (001) sliding would be possible but not easy as in the case of lizardite. This feature probably explains the higher friction coefficient of antigorite with respect to lizardite (easy (001) sliding due to weak interlayer hydrogen bonds) and chrysotile (easy “fibre on fibre” sliding). The relatively high friction coefficient of antigorite indicates that, at least under shallow conditions, slickenfibres dominated by antigorite may be “locked” with respect to chrysotile-dominated faults, and that they could be the sites for possible stick-slip processes.

6. Discussion and Conclusions

Serpentinites play a key role in geodynamics, drastically influencing the physical and mechanical properties of the oceanic and continental crust. Serpentine can start to influence fault mechanics from the onset of peridotite hydration, when only a small amount of serpentine (10–15% of total rock volume) can lead to a significant weakening effect (e.g., [48]). Conversely, serpentine dehydration and breakdown to anhydrous and relatively strong minerals has been linked to fluid overpressure, embrittlement and intermediate-depth seismicity in subduction zones (e.g., [7,9,10]). A key mechanical feature of serpentinites that has been highlighted in recent review articles (e.g., [11,12,14]), is that they are relatively weak under certain P-T conditions. Due to this, serpentinite has been invoked in the initiation of plate tectonics (e.g., [6]), and has been explored as a possible explanation for the aseismic creeping behaviour of fault zones in the oceanic and continental lithosphere (e.g., [3,6,82]). In particular, lithospheric weakening due to serpentinisation results in strain localisation into narrow shear zones and allows for the accommodation of km-scale displacements at slip rates of cm/year [14]. Based on geological and geophysical observations, serpentinites are therefore considered as suitable candidates to explain long-term fault weakness and the creeping behaviour of major tectonic structures [17,38,82].

In this paper, we focused on the mineralogical and microstructural evolution of retrograde pseudomorphic serpentinites, which are the most common type of serpentinite in the oceanic lithosphere, particularly at slow to ultraslow spreading ridges (e.g., [35]). Our observations are in agreement with previous studies that describe serpentinites as weak geological materials, representing suitable candidates for strain localisation.

Recent friction data (Figure 2b and [62]) confirm that undeformed retrograde serpentinites with pseudomorphic textures are significantly weaker (0.3) than anhydrous peridotites and most other common rock types (μ in the Byerlee range of 0.6–0.8; Figure 9a).

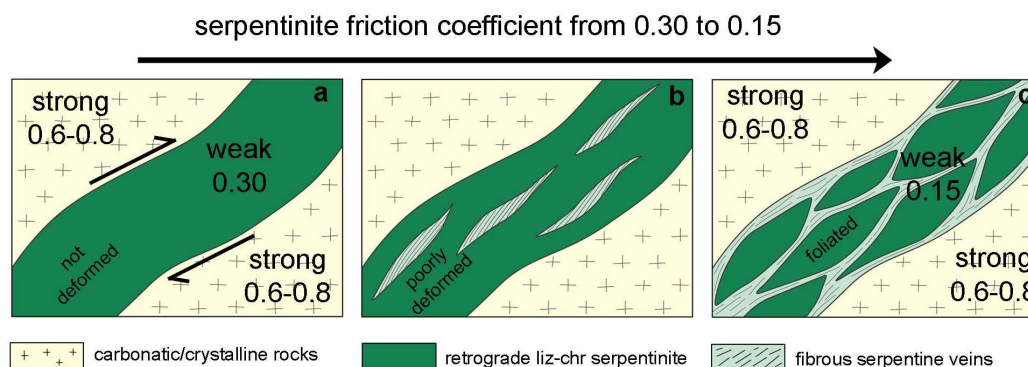


Figure 9. Schematic cartoon of possible evolution of strain localisation and frictional strength in retrograde serpentinites. (a–c) Strain localisation in serpentinites and mechanical evolution from undeformed retrograde serpentinites ($\mu = 0.3$) to foliated, lizardite-rich serpentinites ($\mu = 0.18$), respectively. In (c), the pervasive occurrence of anastomosing ultraweak slickenfaults, mostly formed by chrysotile and polygonal serpentine may result in further weakening ($\mu = 0.15$).

Strain localisation in serpentinite triggers two main processes that feedback into a progressive weakening: (1) pressure solution within massive and foliated serpentinite; and (2) precipitation of new ultraweak serpentines in slickenfault veins/faults. Preferential dissolution of mesh cores and of unfavourably oriented lizardite rims determines the progressive evolution from undeformed retrograde serpentinites ($\mu = 0.3$; Figure 4) to foliated serpentinites (Figure 5). The latter mostly consist of frictionally weak lizardite ($\mu = 0.18$), which forms an interconnected network of subparallel (001) lamellae (lizardite “ribbons” in Figure 5e,f) with (001) planes parallel to shear direction. This microstructure enhances pervasive and easy sliding parallel to (001) basal planes. We therefore expect that the evolution from undeformed to foliated serpentinites with strong CPO may result in further weakening from μ of 0.3 to 0.18. Friction experiments on favourably oriented solid samples of lizardite-rich foliated serpentinite should be performed in the future to verify possible fabric-induced weakening in serpentinites (e.g., [83]).

The other consequence of pressure solution is the precipitation of new serpentine in veins and faults. In most cases, the new material is ultraweak fibrous serpentines ($\mu = 0.15$) consisting of variable proportions of isoriented chrysotile and polygonal serpentines. The evolution from isolated veins (Figure 9b) to interconnected and anastomosing slickenfault veins (Figure 9c) suggests that the overall strength of highly deformed serpentinites could be mostly determined by the weakest domains (i.e. the ultraweak and interconnected slickenfault veins) where deformation is localised. Therefore, the occurrence of both lizardite-rich foliated serpentinites and fibrous slickenfault veins/faults may collectively lead to progressive and substantial weakening of the shear zone (Figure 9c), through the combined effect of pervasive (001) slip in lizardite “ribbons” and “fibre on fibre” slip in fibrous serpentines. If pressure solution and precipitation processes become dominant, serpentinitic rocks may evolve towards “chrysotile schists” (e.g., [19]) in which fibrous serpentine slickenfault veins become dominant over foliated serpentinites.

The weakness and the mechanical evolution of retrograde serpentinites are of particular relevance because these rocks constitute important portions of the oceanic lithosphere and are not restricted to relatively narrow mineralised fault zones. It is well known that circulation of hydrothermal fluids in serpentinite-hosted faults can trigger metasomatic reactions leading to the growth of new minerals such as talc, amphibole, chlorite and smectites, potentially modifying the mechanical behaviour of the fault zone (e.g., [5,32,68]). Some metasomatic minerals, such as talc and smectites, have friction coefficients as low as or lower than chrysotile and lizardite, whereas others, such as amphibole and chlorite, have a higher friction coefficient and may cause local strengthening. Strengthening could

be also caused by local crystallisation of antigorite, as observed in fault rocks from the Rainbow and Menez Hom areas along the Mid-Atlantic Ridge [84] and in splintery veins (as discussed above).

A critical factor is the stability of the different serpentine minerals, since this will determine the depth ranges and the maximum depth at which the weakness of serpentinite is relevant. Based on most published P-T diagrams for serpentine, lizardite and chrysotile are considered to be stable from near-surface conditions up to about 400 °C, although chrysotile may be a “metastable” phase (e.g., [79] and references therein, and [80]). At relatively high temperatures between about 400 and 500 °C, antigorite is thought to be the stable phase. However, geological and petrographic evidence from natural serpentinites clearly indicates that many factors other than pressure and temperature play a critical role in the stability of serpentine minerals (e.g., [85]). In oceanic peridotites, for example, all serpentine minerals can be found over a wide range of temperatures up to 600 °C, with negligible pressure dependence (e.g., [74,79] and references therein). Many authors agree that the occurrence of the different serpentine minerals is mostly controlled by the mode of formation (e.g., precipitation in veins, recrystallisation), reaction kinetics, water/rock ratios and presence of deformation, rather than by P-T conditions alone (e.g., [53,74,79]). For example, Evans [79] suggests that lizardite is the serpentine phase that typically forms during early peridotite hydration over a wide range of temperatures (up to 300 °C), whereas antigorite forms preferentially by replacement of previous serpentines during prograde regional or contact metamorphism at temperatures of 250–600 °C. This is in agreement with Mevel [35], who described the widespread occurrence of lizardite as the first serpentine phase formed by olivine hydration at relatively high temperatures (300–500 °C) based on oxygen isotope fractionation. Therefore, the upper thermal limit of lizardite is probably closer to 500 °C, indicating that this serpentine mineral can no longer be considered as the “low temperature” variety, a conclusion that is in agreement with thermal analyses [86] and high-T deformation experiments [87]. This may have a fundamental geodynamic implication since it expands the temperature and depth range across which the low frictional strength of lizardite and of lizardite-rich retrograde serpentinites may influence fault mechanics.

Author Contributions: Cecilia Viti is the author invited by the editorial staff of this Special Issue and wrote the paper. Cecilia Viti provided the samples and performed the optical microscope and SEM investigations; Cristiano Colletini and Telemaco Tesei contributed to the interpretation of deformation mechanisms and of friction properties of serpentine samples; Steven Smith and Matt Tarling contributed to microstructural observations and to the interpretation of deformation mechanisms. All authors are currently involved in common research projects dealing with serpentine minerals and serpentinite deformation

Acknowledgments: Steven Smith was supported by the Marsden Fund Council (Fast-Start project UOO1417) administered by the Royal Society of New Zealand, and a University of Otago Research Grant. Telemaco Tesei acknowledges the support of the Marie Skłodowska-Curie Fellowship (“STRAIN”, project n° 748400) administered by European Commission.

Conflicts of Interest: The authors declare no conflict of interest.

References

1. Reinen, L.A.; Weeks, J.D.; Tullis, T.E. The frictional behaviour of serpentinite: Implications for aseismic creep on shallow crustal faults. *Geophys. Res. Lett.* **1991**, *18*, 1921–1924. [[CrossRef](#)]
2. Moore, D.E.; Lockner, D.A.; Summers, R.; Shengli, M.; Byerlee, J.D. Strength of chrysotile-serpentinite gouge under hydrothermal conditions: Can it explain a weak San Andreas fault? *Geology* **1996**, *24*, 1041–1044. [[CrossRef](#)]
3. Moore, D.E.; Lockner, D.A.; Summers, R.; Byerlee, J.D.; Ma, S. Sample characterizations and strength measurements of serpentinite gouges. *US Geol. Surv. Open-File Rep.* **1996**, 96–702.
4. Escartin, J.; Hirth, G.; Evans, B.W. Strength of slightly serpentinitized peridotites: Implications for the tectonics of oceanic lithosphere. *Geology* **2001**, *29*, 1023–1026. [[CrossRef](#)]
5. Moore, D.E.; Rymer, M.J. Talc-bearing serpentinite and the creeping section of the San Andreas fault. *Nature* **2007**, *448*, 795–797. [[CrossRef](#)] [[PubMed](#)]

6. Amiguet, E.; Reynard, B.; Caracas, R.; Van de Moortele, B.; Hilariet, N.; Wang, Y.B. Creep of phyllosilicates at the onset of plate tectonics. *Earth Planet. Sci. Lett.* **2012**, *345*, 142–150. [[CrossRef](#)]
7. Peacock, S.M. Are the lower planes of double seismic zones caused by serpentine dehydration in subducting oceanic mantle? *Geology* **2001**, *29*, 299–302. [[CrossRef](#)]
8. Dobson, D.P.; Meredith, P.G.; Boon, S.A. Simulation of subduction zone seismicity by dehydration of serpentine. *Science* **2002**, *298*, 1407–1410. [[CrossRef](#)] [[PubMed](#)]
9. Jung, H.; Green, H.W. Experimental faulting of serpentinite during dehydration: Implications for earthquakes, seismic low-velocity zones, and anomalous hypocenter distributions in subduction zones. *Int. Geol. Rev.* **2004**, *46*, 1089–1102. [[CrossRef](#)]
10. Chollet, M.; Daniel, I.; Koga, K.T.; Morard, G.; van der Moortele, B. Kinetics and mechanism of antigorite dehydration: Implications for subduction zone seismicity. *J. Geophys. Res.* **2011**, *166*, B04203. [[CrossRef](#)]
11. Reynard, B. Serpentine in active subduction zones. *Lithos* **2013**, *178*, 171–185. [[CrossRef](#)]
12. Hirth, G.; Guillot, S. Rheology and tectonic significance of serpentinite. *Elements* **2013**, *9*, 107–113. [[CrossRef](#)]
13. Amiguet, E.; Van De Moortele, B.; Cordier, P.; Hilariet, N.; Reynard, B. Deformation mechanisms and rheology of serpentines in experiments and in nature. *J. Geophys. Res. Solid Earth* **2014**, *119*, 4640–4655. [[CrossRef](#)]
14. Guillot, S.; Schwartz, S.; Reynard, B.; Agard, P.; Prigent, C. Tectonic significance of serpentinites. *Tectonophysics* **2015**, *646*, 1–19. [[CrossRef](#)]
15. Maltman, A.J. Serpentinite textures in Anglesey, North Wales, United Kingdom. *Geol. Soc. Am. Bull.* **1978**, *89*, 972–980. [[CrossRef](#)]
16. Norrel, G.T.; Teixell, A.; Harper, G.D. Microstructure of serpentinite mylonites from the Josephine ophiolite and serpentinitization in retrogressive shear zones, California. *Geol. Soc. Am. Bull.* **1989**, *101*, 673–682. [[CrossRef](#)]
17. Hoogerduijn Strating, E.H.; Visser, R.L.M. Structures in natural serpentinite gouges. *J. Struct. Geol.* **1994**, *16*, 1205–1215. [[CrossRef](#)]
18. Hermann, J.; Muntener, O.; Scambelluri, M. The importance of serpentinite mylonites for subduction and exhumation of oceanic crust. *Tectonophysics* **2000**, *327*, 225–238. [[CrossRef](#)]
19. Andreani, M.; Boullier, A.-M.; Gratier, J.-P. Development of schistosity by dissolution-crystallization in a Californian serpentinite gouge. *J. Struct. Geol.* **2005**, *27*, 2256–2267. [[CrossRef](#)]
20. Auzende, A.-L.; Guillot, S.; Devouard, B.; Baronnet, A. Serpentinites in an Alpine convergent setting: Effects of metamorphic grade and deformation on microstructures. *European J. Miner.* **2006**, *18*, 21–33. [[CrossRef](#)]
21. Hirauchi, K.; Yamaguchi, H. Unique deformation processes involving the recrystallization of chrysotile within serpentinite: Implications for aseismic slip events within subduction zones. *Terra Nova* **2007**, *19*, 454–461. [[CrossRef](#)]
22. Bellot, J.-P. Natural deformation related to serpentinitization of an ultramafic inclusion within a continental shear zone: The key role of fluids. *Tectonophysics* **2008**, *449*, 133–144. [[CrossRef](#)]
23. Raleigh, C.B.; Paterson, M.S. Experimental deformation of serpentinite and its tectonic implications. *J. Geophys. Res.* **1965**, *70*, 3965–3985. [[CrossRef](#)]
24. Escartin, J.; Hirth, G.; Evans, B.W. Nondilatant brittle deformation of serpentinites: Implications for the Mohr-Coulomb theory and the strength of faults. *J. Geophys. Res.* **1997**, *102*, 2897–2913. [[CrossRef](#)]
25. Hirose, T.; Bystricky, M.; Kunze, K.; Stunitz, H. Semi-brittle flow during dehydration of lizardite-chrysotile serpentinite deformed in torsion: Implications for the rheology of oceanic lithosphere. *Earth Planet. Sci. Lett.* **2006**, *249*, 484–493. [[CrossRef](#)]
26. Chernak, L.J.; Hirth, G. Deformation of antigorite serpentinite at high temperature and pressure. *Earth Planet. Sci. Lett.* **2010**, *296*, 23–33. [[CrossRef](#)]
27. Hirauchi, K.; Katayama, I.; Uehara, S.; Miyahara, M.; Takai, Y. Inhibition of subduction thrust earthquakes by low-temperature plastic flow in serpentine. *Earth Planet. Sci. Lett.* **2010**, *295*, 349–357. [[CrossRef](#)]
28. Mugnaioli, E.; Logar, M.; Mellini, M.; Viti, C. Complexity in 15- and 30-sectors polygonal serpentine: Longitudinal sections, intrasector stacking faults, cyclic twins and XRPD satellites. *Am. Miner.* **2007**, *92*, 603–616. [[CrossRef](#)]
29. Andreani, M.; Grauby, O.; Baronnet, A.; Munoz, M. Occurrence, composition and growth of polyhedral serpentine. *European J. Miner.* **2008**, *20*, 159–171. [[CrossRef](#)]

30. Reinen, L.A.; Weeks, J.D.; Tullis, T.E. The frictional behavior of lizardite and antigorite serpentinites: Experiments, constitutive models, and implications for natural faults. *Pure Appl. Geophys.* **1994**, *143*, 317–358. [[CrossRef](#)]
31. Petriglieri, J.R.; Salvioli Mariani, E.; Mantovani, L.; Tribaudino, M.; Lottici, P.P.; Laporte-Magoni, C.; Bersan, D. Micro-Raman mapping of the polymorphs of serpentine. *J. Raman Spectrosc.* **2015**, *46*, 953–958. [[CrossRef](#)]
32. Boschi, C.; Fruh-Green, G.L.; Escartin, J. Occurrence and significance of serpentinite-hosted, talc- and amphibole-rich fault rocks in modern oceanic settings and ophiolite complexes: an overview. *Ophioliti* **2006**, *31*, 129–140.
33. Moore, D.E.; Lockner, D.A. Frictional strengths of talc-serpentine and talc-quartz mixtures. *J. Geophys. Res.* **2011**, *116*, B01403. [[CrossRef](#)]
34. Wicks, F.J.; Whittaker, E.J.W. Serpentine textures and serpentinitization. *Can. Miner.* **1977**, *15*, 459–488.
35. Mevel, C. Serpentinization of abyssal peridotites at mid-ocean ridges. *C. R. Geosci.* **2003**, *335*, 825–852. [[CrossRef](#)]
36. Bonatti, E. Serpentine protrusions in the oceanic crust. *Earth Planet. Sci. Lett.* **1976**, *32*, 107–113. [[CrossRef](#)]
37. Bailey, W.R.; Holdsworth, E.; Swarbrick, R.E. Kinematic history of a reactivated oceanic suture: The Mamonia Complex Suture Zone SW Cyprus. *J. Geol. Soc.* **2000**, *157*, 1107–1126. [[CrossRef](#)]
38. Coleman, R.G. Petrologic and geophysical nature of serpentinites. *Geol. Soc. Am. Bull.* **1971**, *82*, 897–918. [[CrossRef](#)]
39. Irwin, W.P.; Barnes, I. Effects of geological structure and fluids on the seismic behaviour of the San Andreas fault system in central and northern California. *Geology* **1975**, *3*, 713–716. [[CrossRef](#)]
40. Dilek, Y. Ophiolite concept and its evolution. *Spec. Papers-Geol. Soc. Am.* **2003**, 1–16.
41. Auzende, A.-L.; Escartin, J.; Walte, N.P.; Guillot, S.; Hirth, G.; Frost, D.J. Deformation mechanisms of antigorite serpentinite at subduction zone conditions determined from experimentally and naturally deformed rocks. *Earth Planet. Sci. Lett.* **2015**, *411*, 229–240. [[CrossRef](#)]
42. Picazo, S.; Manatschal, G.; Cannat, M.; Andreani, M. Deformation associated to exhumation of serpentinitized mantle rocks in a fossil ocean continent transition: The Totalp unit in SE Switzerland. *Lithos* **2013**, *176*, 255–271. [[CrossRef](#)]
43. Wicks, F.J. Deformation histories as recorded by serpentinites. II Deformation during and after serpentinitization. *Can. Miner.* **1984**, *22*, 197–203.
44. Plümer, O.; Røyne, A.; Magrasó, A.; Jamtveit, B. The interface-scale mechanism of reaction-induced fracturing during serpentinitization. *Geology* **2012**, *40*, 1103–1106.
45. O’Hanley, D.S. Solution to the volume problem in serpentinitization. *Geology* **1992**, *20*, 705–708.
46. Iyer, K.; Jamtveit, B.; Mathiesen, J.; Malthe-Sørenssen, A.; Feder, J. Reaction-assisted hierarchical fracturing during serpentinitization. *Earth Planet. Sci. Lett.* **2008**, *267*, 503–516. [[CrossRef](#)]
47. Jamtveit, B.; Malthe-Sørenssen, A.; Kostenko, O. Reaction enhanced permeability during retrogressive metamorphism. *Earth Planet. Sci. Lett.* **2008**, *267*, 620–627. [[CrossRef](#)]
48. Escartin, J.; Hirth, G.; Evans, B.W. Effects of serpentinitization on the lithospheric strength and the style of normal faulting at slow-spreading ridges. *Earth Planet. Sci. Lett.* **1997**, *151*, 181–189. [[CrossRef](#)]
49. Campione, M.; Capitani, G. Subduction-zone earthquake complexity related to frictional anisotropy in antigorite. *Nat. Geosci.* **2013**, *6*, 847–851. [[CrossRef](#)]
50. Page, B.M.; De Vito, L.A.; Coleman, R.G. Tectonic emplacement of serpentinite southeast of San Jose, California. *Int. Geol. Rev.* **1999**, *41*, 494–505. [[CrossRef](#)]
51. Wassmann, S.; Stöckhert, B.; Trepmann, C.A. Dissolution precipitation creep versus crystalline plasticity in high-pressure metamorphic serpentinites. In *Deformation Mechanisms, Rheology and Tectonics: Microstructures, mechanics and Anisotropy*; Prior, D.J., Rutter, E.H., Tatham, D.J., Eds.; Geology Society Special Publication: London, UK, 2011; Volume 360, pp. 129–149.
52. Padron-Navarta, J.A.; Tommasi, A.; Garrido, C.J.; Lopez Sanchez-Vizcaino, V. Plastic deformation and development of antigorite crystal preferred orientation in high-pressure serpentinites. *Earth Planet. Sci. Lett.* **2012**, *349*, 75–86. [[CrossRef](#)]
53. Andreani, M.; Baronnet, A.; Boullier, A.-M.; Gratier, J.-P. A microstructural study of a “crack-seal” type serpentine vein using SEM and TEM techniques. *Eur. J. Miner.* **2004**, *16*, 585–595. [[CrossRef](#)]
54. Kawano, S.; Katayama, I.; Okazaki, K. Permeability anisotropy of serpentinite and fluid pathways in a subduction zone. *Geology* **2011**, *39*, 939–942. [[CrossRef](#)]

55. Katayama, I.; Terada, T.; Okazaki, K.; Tanikawa, W. Episodic tremor and slow slip potentially linked to permeability contrasts at the Moho. *Nat. Geosci.* **2012**, *5*, 731–734. [[CrossRef](#)]
56. Schwarzenbach, E.M. Serpentinization and the formation of fluid pathways. *Geology* **2016**, *44*, 175–176. [[CrossRef](#)]
57. Tutolo, B.M.; Mildner, D.F.R.; Gagnon, C.V.L.; Saar, M.O.E.; Seyfried, W.E., Jr. Nanoscale constraints on porosity generation and fluid flow during serpentinization. *Geology* **2016**, *44*, 103–106. [[CrossRef](#)]
58. Moore, D.E.; Lockner, D.A.; Shengli, M.; Summers, R.; Byerlee, J.D. Strengths of serpentinite gouges at elevated temperatures. *J. Geophys. Res.* **1997**, *102*, 14787–14801. [[CrossRef](#)]
59. Behnsen, J.; Faulkner, D. Frictional strength of sheet silicates under medium to high pressure. *J. Struct. Geol.* **2012**, *42*, 49–61. [[CrossRef](#)]
60. Moore, D.E.; Lockner, D.A.; Tanaka, H.; Iwata, K. The coefficient of friction of chrysotile gouge at seismogenic depths. *Int. Geol. Rev.* **2004**, *46*, 385–398. [[CrossRef](#)]
61. Dengo, C.A.; Logan, J.M. Implications of the mechanical and frictional behavior of serpentinite to seismogenic faulting. *J. Geophys. Res.* **1981**, *86*, 10771–10782. [[CrossRef](#)]
62. Tesei, T.; Harbord, C.W.; Collettini, C.; De Paola, N.; Viti, C. Friction of lizardite and fibrous serpentine: implications for the weakness of major serpentine-bearing faults. *J. Geophys. Res.* (under review).
63. Takahashi, M.; Uehara, S.; Mizoguchi, K.; Shimizu, I.; Okazaki, K.; Masuda, K. On the transient response of serpentine (antigorite) gouge to stepwise changes in slip velocity under high-temperature conditions. *J. Geophys. Res.* **2011**, *116*, B10405. [[CrossRef](#)]
64. Reinen, L.A.; Tullis, T.E. Microstructural evidence of strain localization and distributed strain in serpentinite friction experiments. *Eos Trans. AGU* **1995**, *76*, 560.
65. Moore, D.E.; Lockner, D.A. Crystallographic controls on the frictional behavior of dry and water-saturated sheet structure minerals. *J. Geophys. Res.* **2004**, *109*, B03401. [[CrossRef](#)]
66. Morrow, C.A.; Moore, D.E.; Lockner, D.A. The effect of mineral bond strength and adsorbed water on fault gouge frictional strength. *Geophys. Res. Lett.* **2000**, *27*, 815–818. [[CrossRef](#)]
67. Wibberley, C. Talc at fault. *Nature* **2007**, *448*, 756–757. [[CrossRef](#)] [[PubMed](#)]
68. Sone, H.; Shimamoto, T.; Moore, D.E. Frictional properties of saponite-rich gouge from a serpentinite-bearing fault zone along the Gokasho-Arashima Tectonic Line, central Japan. *J. Struct. Geol.* **2011**, *38*, 172–182. [[CrossRef](#)]
69. Viti, C.; Mellini, M. Vein antigorites from Elba Island, Italy. *Eur. J. Miner.* **1996**, *8*, 423–434. [[CrossRef](#)]
70. Viti, C.; Mellini, M. Contrasting chemical compositions in associated lizardite and chrysotile in veins from Elba, Italy. *Eur. J. Miner.* **1997**, *9*, 585–596. [[CrossRef](#)]
71. Viti, C.; Mellini, M. Mesh textures and bastites in the Elba retrograde serpentinites. *Eur. J. Miner.* **1998**, *10*, 1341–1359. [[CrossRef](#)]
72. Marroni, M.; Pandolfi, L. The architecture of an incipient oceanic basin: a tentative reconstruction of the Jurassic Liguria-Piemonte basin along the Northern Apennines-Alpine Corsica transect. *Int. J. Earth Sci.* **2007**, *96*, 1059–1078. [[CrossRef](#)]
73. Carmignani, L.; Conti, P.; Cornamusini, G.; Pirro, A. Geological map of Tuscany. *J. Maps* **2013**, *9*, 487–497. [[CrossRef](#)]
74. Andreani, M.; Mevel, C.; Boullier, A.-M.; Escartin, J. Dynamic control on serpentine crystallization in veins: Constraints on hydration processes in oceanic peridotites. *Geochem. Geophys. Geosystems* **2007**, *8*. [[CrossRef](#)]
75. Groppo, C.; Compagnoni, R. Ubiquitous fibrous antigorite veins from the Lanzo Ultramafic Massif, Internal western Alps (Italy): Characterisation and genetic conditions. *Period. Miner.* **2007**, *76*, 169–181.
76. Quesnel, B.; Gautier, P.; Cathelineau, M.; Boulvais, P.; Couteau, C.; Drouillet, M. The internal deformation of the Peridotite Nappe of New Caledonia: A structural study of serpentine-bearing faults and shear zones in the Koniambo Massif. *J. Struct. Geol.* **2016**, *85*, 51–67. [[CrossRef](#)]
77. Bortolotti, V.; Fazzuoli, M.; Pandeli, E.; Principi, G.; Babbini, A.; Corti, S. Geology of Central and Eastern Elba Island, Italy. *Ofioliti* **2001**, *26*, 97–150.
78. Mellini, M.; Trommsdorff, V.; Compagnoni, R. Antigorite polysomatism: Behaviour during progressive metamorphism. *Contrib. Miner. Pet.* **1987**, *97*, 147–155. [[CrossRef](#)]
79. Evans, B.W. The serpentinite multisystem revised: chrysotile is metastable. *Int. Geol. Rev.* **2004**, *46*, 479–506. [[CrossRef](#)]
80. Evans, B.W.; Hattori, K.; Baronnet, A. Serpentinite: what, why, where? *Elements* **2013**, *9*, 99–106. [[CrossRef](#)]

81. McCaig, A.M.; Delacour, A.; Fallick, A.E.; Castelain, T.; Fruh-Green, G.L. Detachment fault control on hydrothermal circulation systems: Interpreting the subsurface beneath the TAG hydrothermal field using the isotopic and geological evolution of oceanic core complexes in the Atlantic. In *Diversity of Hydrothermal Systems on Slow-Spreading Ocean Ridges, In Proceeding of 2010 AGU Fall Meeting, San Francisco, CA, USA, 13–17 December 2010*; Rona, P.A., Devey, C., Dymont, J., Murton, B., Eds.; AGU Publications: Washington, DC, USA, 2010; Volume 108, pp. 207–239.
82. Hilariet, N.; Reynard, B.; Wang, Y.; Daniel, I.; Merkel, S.; Nishiyama, N.; Petitgirard, S. High-pressure creep of serpentine, interseismic deformation and initiation of subduction. *Science* **2007**, *318*, 1910–1913. [[CrossRef](#)] [[PubMed](#)]
83. Collettini, C.; Niemeijer, A.; Viti, C.; Marone, C. Fault zone fabric and fault weakness. *Nature* **2009**, *462*, 907–911. [[CrossRef](#)] [[PubMed](#)]
84. Ribeiro Da Costa, I.; Barriga, F.J.A.S.; Viti, C.; Mellini, M.; Wicks, F.J. Antigorite in deformed serpentinites from the Mid-Atlantic Ridge. *Eur. J. Miner.* **2008**, *20*, 563–572. [[CrossRef](#)]
85. Schwartz, S.; Guillot, S.; Reynard, B.; Lafay, R.; Debret, B.; Nicollet, C.; Lanari, P.; Auzende, A.L. Pressure-temperature estimates of the lizardite/antigorite transition in high pressure serpentinites. *Lithos* **2013**, *178*, 197–210. [[CrossRef](#)]
86. Viti, C. Serpentine minerals discrimination by thermal analysis. *Am. Mineral.* **2010**, *95*, 631–638. [[CrossRef](#)]
87. Viti, C.; Hirose, T. Dehydration reactions and micro-nanostructures in experimentally-deformed serpentinites. *Contrib. Miner. Pet.* **2009**, *157*, 327–338. [[CrossRef](#)]



© 2018 by the authors. Licensee MDPI, Basel, Switzerland. This article is an open access article distributed under the terms and conditions of the Creative Commons Attribution (CC BY) license (<http://creativecommons.org/licenses/by/4.0/>).